Influence of Inelastic Scattering at Metal-Dielectric Interfaces

Patrick E. Hopkins

Pamela M. Norris[1]
e-mail: pamela@virginia.edu

Department of Mechanical and Aerospace Engineering,
University of Virginia,
P.O. Box 400746,
Charlottesville, VA 22904-4746

Robert J. Stevens
Department of Mechanical Engineering,
Rochester Institute of Technology,
76 Lomb Memorial Drive,
Rochester, NY 14623-5604

Thermal boundary conductance is becoming increasingly important in microelectronic device design and thermal management. Although there has been much success in predicting and modeling thermal boundary conductance at low temperatures, the current models applied at temperatures more common in device operation are not adequate due to our current limited understanding of phonon transport channels. In this study, the scattering processes across Cr/Si, Al/Al_2O_3, Pt/Al_2O_3, *and* Pt/AlN *interfaces were examined by transient thermoreflectance testing at high temperatures. At high temperatures, traditional models predict the thermal boundary conductance to be relatively constant in these systems due to assumptions about phonon elastic scattering. Experiments, however, show an increase in the conductance indicating inelastic phonon processes. Previous molecular dynamic simulations of simple interfaces indicate the presence of inelastic scattering, which increases interfacial transport linearly with temperature. The trends predicted computationally are similar to those found during experimental testing, exposing the role of multiple-phonon processes in thermal boundary conductance at high temperatures.* [DOI: 10.1115/1.2787025]

Keywords: thermal boundary conductance, diffuse mismatch model, inelastic scattering, nanoscale, solid interfaces

Introduction

The ongoing trend of miniaturization of devices with structures on nanometer length scales has given rise to new challenges in the science and engineering of thermal transport and management. As these length scales continue to decrease, heat transport around active regions in these devices is enhanced/restricted by interfaces between materials and the structures surrounding them. Therefore, the issue of thermal management is becoming more critical in device engineering and reliability [1], particularly in thermoelectrics [2,3], thin-film high temperature superconductors [4,5], vertical cavity surface emitting lasers [6], and optical data storage media [7]. An ever increasing challenge in the development of these devices is successfully accounting for the temperature drop ΔT across the interface caused by, for example, the transport properties of the different materials [8], the presence of gaps and voids in the lattice structure due to nonperfect contacts [2], or a disordered region of the materials resulting from device fabrication conditions [9]. In any case, this temperature drop is characterized by the thermal boundary conductance h_{BD} which is the conductance per unit area that relates the heat flux across the interface, q_{BD}, to the temperature drop ΔT across the interface. This is mathematically expressed as $q_{BD}=h_{BD}\Delta T$.

Background

An understanding of the basic transport mechanisms involved in thermal boundary conductance is critical to the design and engineering of nanostructured devices. The main resistance to interfacial transport in the majority of these devices is phonon scattering between two materials, which has been successfully predicted by various models in limiting cases. Little proposed the acoustic mismatch model (AMM) to account for the specular scattering of phonons at an interface between two materials at low temperatures [10,11]. The root of the AMM theory is the wave nature of phonon transport. At low temperatures (when the dominant phonon wavelength is long) and at perfect interfaces, an incident phonon at a boundary of two materials can be treated as a plane wave, and the reflection and transmission probabilities can be analyzed similar to that of photons (Snell's law) [10,11]. This approach assumes that the phonon is transmitted or reflected at the interface (not scattered), an assumption that is valid when predicting h_{BD} at low temperatures ($T<7$ K) and at ideal interfaces where specular scattering is probable [9]. However, this ideal case only represents a very limited population of interfaces in modern devices, which may operate at higher temperatures and have disordered regions near the interface that would induce diffuse scattering. To account for this type of phonon scattering, Swartz and Pohl developed the diffuse mismatch model (DMM) to predict h_{BD} at more realistic interfaces [12].

The DMM provides a quick and simple estimation of h_{BD} for an interface between the two materials [12]. To apply the DMM in its simplest form, the following assumptions must be made [13]: (1) phonons are elastically scattered, i.e., when a phonon from Side 1 with frequency ω scatters at the interface, it can only emit a phonon into Side 2 with the same frequency ω (for discussions, Side 1 will refer to the softer material with lower phonon velocities and Side 2 will refer to the stiffer material with higher phonon velocities); (2) phonon scattering is completely diffuse, i.e., a scattered phonon has no memory of the mode (longitudinal or transverse) or direction of the incident phonon; and (3) the materials on both sides of the interface are elastically isotropic, i.e., the longitudinal and transverse acoustic velocities are constant in all crystallographic directions. This model has been shown to predict conductance across higher temperature interfaces ($T>15$ K) relatively well [9,12]. However, at much higher temperatures (as T approaches T_{room}), the DMM has been shown to either underpredict or overpredict experimental data, depending on the material systems [8,13–15]. The overprediction of the DMM has been associated with multiple elastic scattering events occurring from material mixing around the boundary in materials systems where the Debye temperature, θ_D, of both materials is greater than T_{room} [16–19]. The underprediction of the DMM in material systems where θ_D of one material is less than T_{room} has been attributed to inelastic phonon scattering processes, which is the focus of this paper.

[1]Corresponding author.

Contributed by the Heat Transfer Division of ASME for publication in the JOURNAL OF HEAT TRANSFER. Manuscript received July 24, 2006; final manuscript received June 14, 2007; published online February 4, 2008. Review conducted by Suresh V. Garimella.

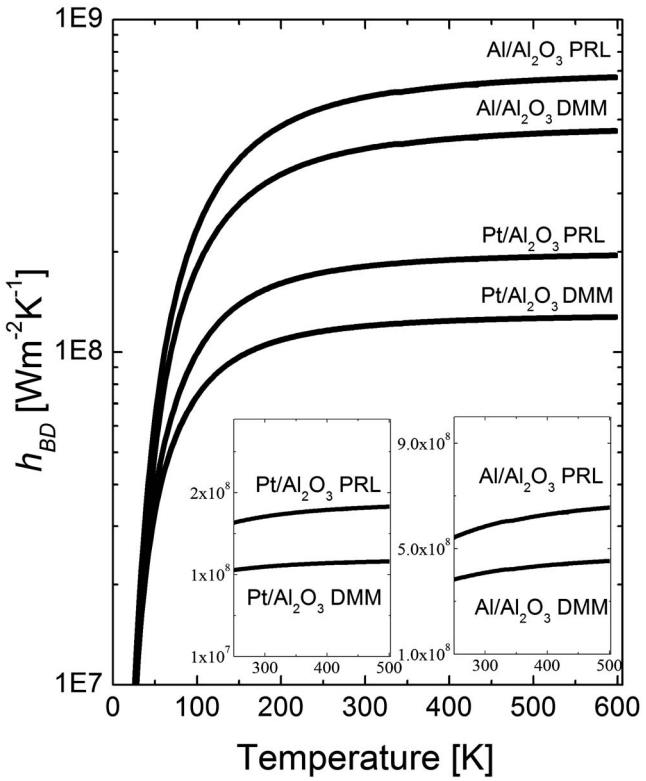

Fig. 1 Thermal boundary conductance calculations of the Al/Al_2O_3 and Pt/Al_2O_3 interfaces using DMM and PRL. The models level off at higher temperatures due to the assumption of elastic scattering used in the calculations. The inset graphs show the DMM and PRL for the materials systems over only the temperature range used in this work.

Another model for h_{BD}, the phonon radiation limit (PRL), provides a quick and simple determination of the maximum conductance for interfacial transport assuming complete elastic scattering [20]. Calculations of the PRL assume that phonons from Side 2 with frequencies below the cutoff frequency of Side 1 transmit completely to Side 1 [15]. The results of the DMM and PRL for Al/Al_2O_3 and Pt/Al_2O_3 interfaces are shown in Fig. 1 with parameters listed in Table 1. Since the PRL represents the upper limit of the elastic contribution to thermal transport, it will always predict a higher h_{BD} than the DMM. Notice that the DMM and PRL predict a constant h_{BD} at temperatures approaching θ_D in each material. The insets of Fig. 1 show a close-up of the DMM and PRL calculations for the two material systems over the temperature range used in this study.

In an attempt to investigate the underpredictive trends in h_{BD} of the DMM and PRL, several computational and experimental efforts have been undertaken. In 1993, Stoner and Maris reported h_{BD} at a range of acoustically mismatched interfaces from 50 K to 300 K [15,21]. As expected from the DMM, the measured h_{BD} decreased with an increase in sample mismatch and the change in h_{BD} decreased with temperature. In the sample with the greatest mismatch, Pb/diamond (Table 1), values of h_{BD} were measured that exceeded the DMM prediction by over an order of magnitude, however, the measured h_{BD} remained fairly constant over the temperature range investigated, which does not agree with the T^3 trend of the DMM at low temperatures. This measurement also significantly exceeded the prediction of the PRL. One possible explanation offered for this relatively large h_{BD} was the occurrence of inelastic scattering—i.e., one or more phonons of frequency ω_1 on Side 1 were emitting one or more phonons of frequency ω_2 on Side 2—thereby offering more channels for transport than the DMM and PRL account for, leading to an underestimate of h_{BD} by the DMM and PRL. For the Pb/diamond case, a high frequency diamond phonon could scatter at the interface and emit several low frequency phonons on the Pb side.

Chen et al. recently used molecular dynamics (MD) simulations to show a linear increase in h_{BD} across a Kr/Ar nanowire with an increase in temperature from 35 K to 55 K, which they ascribed to anharmonic processes [22]. Kosevich considered the role of inelastic scattering on the phonon transmission probability [23]. With a multiharmonic model, Kosevich was able to show that inelastic scattering makes a greater contribution to h_{BD} than elastic scattering for interfaces with very different vibrational spectra; these calculations, however, were not material specific. Observation of inelastic scattering in specific material systems applicable in microelectronic systems has not been predicted theoretically or computationally, and has been shown experimentally by Lyeo and Cahill only at low temperatures ($T \leqslant T_{room}$) [24]. They observed an approximately linear increase in h_{BD} over a temperature range of 80–300 K on carefully prepared Pb and Bi thin films on diamond substrates with a pump-probe thermoreflectance technique. Like Stoner and Maris, Lyeo and Cahill observed h_{BD} that was several times higher than the PRL but with a linear increase with temperature matching the aforementioned simulation results that suggested that multiple-phonon processes (inelastic scattering) can play a significant role in interface thermal conductance.

The purpose of this study is to examine the temperature dependence of h_{BD} at temperatures around and above θ_D. This research examines the assumption of phonon elastic scattering through measurements of h_{BD} at increased temperatures ($T > T_{room}$) on a range of interfaces comprised of materials with varying θ_D. Previous MD simulations show evidence of what could be inelastic phonon scattering occurring at the interface due to increased temperature. Stevens et al. observed thermal transport across the interface of two fcc lattice systems with varying degrees of mass and lattice mismatch at temperatures in the classical limit [25].

In the classical limit (for real materials $T \gg \theta_D$), h_{BD} calculated by either the DMM or PRL is independent of temperature. The only temperature dependent part of both models is in the distribution function, which at temperatures well above the Debye temperature becomes constant. Because these models do not assume any inelastic scattering, the transmission coefficient is independent of temperature at high temperatures. To check the tempera-

Table 1 Pertinent parameters for DMM and PRL calculations [27,43–45]

Material	θ_D (K)	ν_l (m s^{-1})	ν_t (m s^{-1})	ρ (kg m^{-3})	M (kg mol^{-1})
Al	428	6,240	3,040	2,700	0.027
Cr	630	6,980	4,100	7,190	0.052
Pb	105	2,350	970	11,590	0.207
Pt	240	4,174	1,750	21,620	0.195
Diamond	2,230	17,500	12,800	3,512	0.012
Al_2O_3	1,043	10,890	6,450	3,970	0.102
AlN	1,150	11,120	6,267	3,255	0.02
Si	645	8,970	5,332	2,330	0.028

ture dependence of h_{BD}, Stevens et al. conducted several simulations at a range of temperatures [25]. The simulations were conducted on both highly and lightly mismatched interfaces with Debye temperature ratios of 0.2 and 0.5.

A strong linear relationship was observed in the results of the MD calculations and h_{BD} varied by nearly a factor of 4 for both interfaces for the temperature range considered. The strong linear dependence indicated that there is some thermal transport mechanism that is dependent on temperature, which would lead to a larger transmission coefficient. The most likely explanation for this discrepancy is that the DMM and PRL account only for elastic scattering, while MDS accounts for both elastic and inelastic scattering at the interface. The linear temperature dependence indicates a scattering process that is proportional to phonon population, since the phonon population increases linearly with temperature at high temperatures. In the classical limit, at temperatures above the Debye temperature, it appears that inelastic scattering provides the major contribution to the energy transport across the interface, surpassing the contribution of the elastic scattering.

In an effort to experimentally verify the results of the MD calculations, in this paper, the trends in h_{BD} predicted by both the DMM and PRL are compared to experimental data from film/substrate samples of Cr/Si, Al/Al_2O_3, Pt/Al_2O_3, and Pt/AlN over a temperature range of 293–500 K obtained using the transient thermoreflectance (TTR) technique [26]. By increasing the temperature to levels near and above the Debye temperatures of the metals in these samples, the majority of the film's phonon populations were excited. Assuming elastic scattering, a phonon from the film will scatter at the interface and emit a phonon with the same frequency into the substrate, and a continued increase in temperature above θ_D should not significantly affect h_{BD} since the change in the phonon population in the film is constant. However, results show a continued increase in h_{BD} above the film's θ_D indicating that the change in the substrate phonon population, which is changing at a much faster rate than that of the film in the low θ_D film/high θ_D substrate systems studied in this work, is affecting the h_{BD} via inelastic scattering events: A high frequency phonon in the substrate is scattering at the interface and breaking down into several low frequency phonons in the film.

Experimental Considerations

Samples. Since the goal of this study is to examine the ability of the DMM and PRL (with their elastic scattering assumptions) to predict h_{BD} at high temperatures, materials systems were chosen to encompass different regimes in which the degree of temperature dependence of h_{BD} as predicted by the DMM would vary. Four materials systems were considered (θ_D film, θ_D film/substrate ratio (ξ)) [27]: Cr/Si (630 K, 0.98), Al/Al_2O_3 (428 K, 0.41), Pt/Al_2O_3 (240 K, 0.23), and Pt/AlN (240 K, 0.21). These materials systems allow investigation in temperature regimes where various trends in h_{BD} are predicted by DMM and PRL. For example, assuming elastic scattering, some increase in h_{BD} is expected in the Al/Al_2O_3 samples over most of the temperature range in this study (293–500 K) because the phonon population in Al will increase until $T > \theta_{D\_Al}$. However, in Pt/Al_2O_3, where $\theta_{D\_Pt} < T_{room}$, the increase in h_{BD} should be relatively negligible since the entire Pt phonon population is excited below room temperature. Any increase in h_{BD} when $T > \theta_{D\_Pt}$ could be evidence of more high frequency Al_2O_3 phonons exciting from the elevated temperature, scattering at the interface, and breaking down into two or more lower frequency phonons emitted into the Pt film.

The Cr, Al, and Pt film thicknesses were 50 nm, 75 nm, and 50 nm, respectively, chosen ~50% larger than the electron mean free path in these metals to minimize ballistic electron scattering at the boundary and to ensure that the electrons and phonons in the film have completely equilibrated by the time they reach the interface [28]. These thicknesses were also necessary to ensure that viable h_{BD} information can be obtained from the TTR data from our experimental setup [8]. The Cr was deposited on an *n*-type Ph doped (100) Si substrate; the Al and Pt films were deposited on factory polished Al_2O_3, and an additional Pt film was deposited on factory polished AlN. The metals were deposited on their respective substrates in a multisource, high vacuum thin-film sputter deposition system, a Supersystem III manufactured by the Kurt J. Lesker Company capable of pumping down to 10^{-7} Torr. All substrates were (ETM) spin cleaned with reagent alcohol (90.7% ethyl alcohol; 4.8% isopropyl alcohol; 4.5% methyl alcohol; 0.12% water), trichloroethylene, and methanol, and then subsequently baked for 5 min at 400 K to remove any residual water that may have formed at the substrate surface as a result of the spin clean. The substrates were subject to a 5 min, 100 W backsputter etch, prior to film deposition, in an effort to remove the majority of the native oxide layer and any additional contaminants.

Experimental Setup. The TTR data were taken with the pump-probe experimental setup depicted in Fig. 2. The primary output of the laser system emanates from a Coherent RegA 9000 amplifier operating at a 250 kHz repetition rate with about 4 μJ/pulse and a 150 fs pulse width at 800 nm. The pulses were split at a 9:1 pump to probe ratio. The pump beam, modulated at 125 kHz, was focused down to a 100 μm radius spot size to achieve 10 J m^{-2} fluence. The probe beam was focused to the middle of the pump beam to achieve a pump to probe fluence ratio of 10:1. The radii of the pump and probe beams were measured with a sweeping knife edge [29]. Although the low repetition rate of the RegA system and the "one shot on-one shot off" modulation rate of the pump beam ensure minimal residual heating between pump pulses, the phase of the signal must still be taken into account. Phase correction was performed by the procedures for signal phase adjustment outlined in the references [29].

For the longer scans analyzed in this study (~1400 ps pump-probe delay), alignment of the pump and probe spots can become an issue [8,30]. To avoid misalignment problems, the probe beam was collimated before the probe delay stage and profiled with a sweeping knife edge at all time delays. In this study, a pump to probe radius ratio of 10:1 was used, and the probe was aligned with the delay stage resulting in less than 1.5 μm and 4.0 μm drift along the horizontal and vertical axes perpendicular to the surface, respectively. These spot characteristics result in less than 1% error due to misalignment of the beams [29].

The samples were mounted to a 5 mm thick Al plate attached to a Minco 5419 silicon rubber resistive heater. The samples were mounted on the front of the Al plate with Molykote 44 high temperature vacuum grease to reduce thermal resistance and the sides and back of the aluminum plate/heater were insulated with high temperature millboard insulation. Holes were drilled 1 mm underneath the front surface of the Al plate in four locations surrounding the sample and the temperature of the sample was monitored with Omega Engineering TT-T-20 thermocouple wires with NMP-U-M thermocouple male connectors. For each desired temperature, the Al block was heated and held at constant temperature for ~2 h to ensure that the sample/Al block system equilibrated before TTR measurements were taken. Since the thermal resistance between the Al block and the sample is much less than the thermal resistance between the sample surface and the ambient, it was valid to assume that the Al block and sample were at close temperatures. After several measurements at a certain temperature, the heater was turned off and the system returned to room temperature. Room temperature measurements were again taken and these measurements were compared to ensure that the sample was not damaged as a result of the heating. The value of h_{BD} was determined by fitting the TTR data to the thermal model discussed in the next section. Repeatable results were found at all temperatures. The data presented in this paper are the statistical averages of the data at each temperature. Five to seven data sets were taken

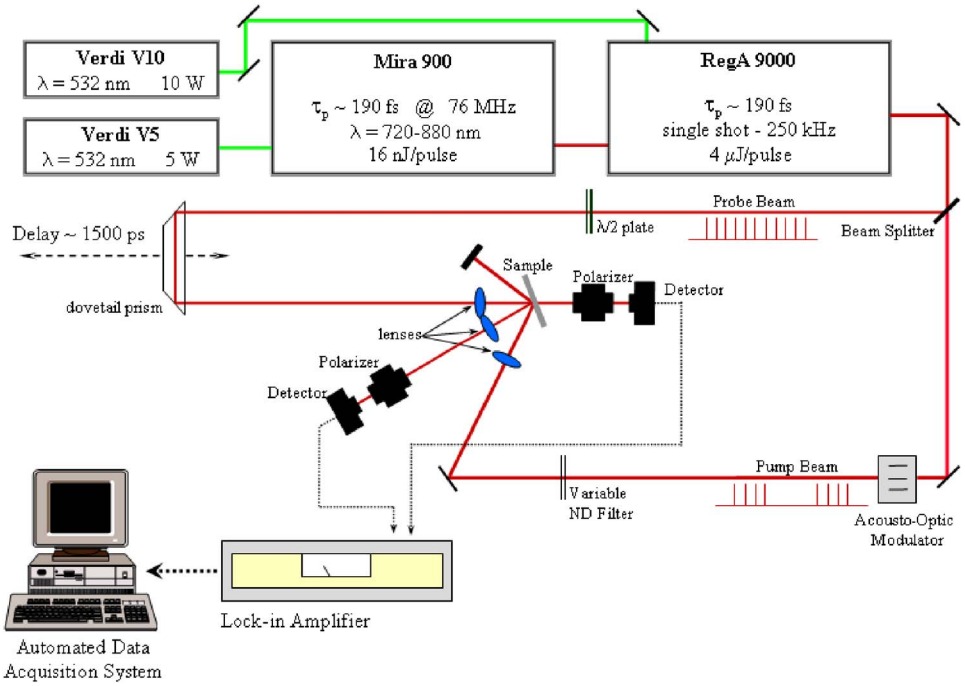

Fig. 2 TTR setup

at each temperature increment. A maximum deviation of 18% from the mean was calculated for the Cr/Si samples, and less than 10% was determined for the other systems.

Thermal Model. The TTR technique produces some excitation of the metal film followed by a cooling of the film due to the film's thermal connection to the substrate. To simplify data reduction, ideally the temperature response is influenced only by conductance across the interface and not by diffusion within the metal film. If the film is too thick or has a low thermal conductivity, however, then there will be two free parameters (film thermal conductivity k_f and h_{BD}) when fitting experimental data to a thermal model. To avoid this situation, the Biot number, Bi, for the interface should be significantly less than 1 (typically less than 0.1) so that the film can be treated as a lumped thermal capacitance [31]. Therefore, the film thickness should be restricted to

$$\mathrm{Bi} = \frac{h_{BD} d}{k_f} < 0.1 \Rightarrow d < \frac{0.1 k_f}{h_{BD}} \tag{1}$$

where d is the film thickness. A more detailed analysis of this assumption for each sample using values measured for h_{BD} will be presented later.

Assuming the metal film can be treated as a lumped capacitance (i.e., Eq. (1) holds), the thermal model for the film and substrate system is

$$\rho d C_f \frac{dT_f(t)}{dt} = h_{BD}[T(0,t) - T_f(t)] \tag{2}$$

$$\frac{\partial T_s(x,t)}{\partial t} = \alpha_s \frac{\partial^2 T_s(x,t)}{\partial x^2} \tag{3}$$

where T_f is the temperature of the film that is measured using the TTR technique, T_s is the substrate temperature and is a function of time and space, and ρ, C_f, and α_s are the film density, film specific heat, and substrate diffusivity, respectively. Radiative and convective losses at the front of the film surface are negligible compared to a typical interface conductance of 10^6–10^8 W m^{-2} K^{-1} and are therefore neglected. The temperatures in Eqs. (2) and (3) can be nondimensionalized by

$$\varphi_{f,s} = \frac{T_{f,s} - T_0}{T_f(0) - T_0} \tag{4}$$

where T_0 is the temperature of the film and substrate immediately before excitation and $T_f(0)$ is the temperature of the film immediately after excitation. Therefore, the thermal model can be expressed as

$$\frac{d\varphi_f(t)}{dt} = \frac{h_{BD}}{\rho d C_f}[\varphi_s(0,t) - \varphi_f(t)] \tag{5}$$

$$\frac{\partial \varphi_s(x,t)}{\partial t} = \alpha_s \frac{\partial^2 \varphi_s(x,t)}{\partial x^2} \tag{6}$$

subject to the following initial conditions:

$$\varphi_f(0) = 1 \tag{7}$$

$$\varphi_s(x,0) = 0 \tag{8}$$

and the following boundary conditions:

$$-k_s \frac{\partial \varphi_s(0,t)}{\partial x} = h_{BD}[\varphi_f(t) - \varphi_s(0,t)] \tag{9}$$

$$\frac{\partial \varphi_s(\infty,t)}{\partial x} = 0 \tag{10}$$

The semi-infinite assumption made in Eq. (10) is reasonable for the time scale of interest, ~1.5 ns. The thermal penetration depth for most substrates at this time scale is $(\alpha_s t)^{1/2} < 1$ μm, which is significantly smaller than the thickness of the substrates used in this study.

Equations (5) and (6) subject to Eqs. (7)–(10) were numerically solved using the Crank–Nicolson method, which has only a second order truncation error in both time and space. The thermal boundary conductance was determined by fitting the TTR data to the model using the material constants listed in Table 2. The models fit to Al/Al_2O_3 and Pt/Al_2O_3 TTR data taken at room and elevated temperatures are shown in Fig. 3. General assumptions and fitting sensitivity of this model are discussed in detail in the

Table 2 Thermophysical properties used in determining h_{BD} from Eqs. (5)–(10) (values listed are at room temperature (T_{room}=293 K). Note the film thermal conductivity is not needed for the lumped capacitance analysis, but is needed for thermal diffusion time approximations. Higher temperature values that were used can be found in the references [31,36,43–45]).

Material	C_L (J m^{-3} K^{-1})	k (W m^{-1} K^{-1})
Al	2.44×10^6	237
Cr	3.3×10^6	93.7
Pt	2.83×10^6	73
Al_2O_3	3.25×10^6	18
AlN	1.94×10^6	285
Si	1.66×10^6	148

references [8,15]. Note that the high temperature data, which have a higher h_{BD} than the low temperature data, show a greater curvature in the exponential decay. In addition, note that the trends in the early part of the data do not match the trends predicted by the thermal model. This occurs in the first 30 ps after laser heating in the Al sample and 70 ps after laser heating in the Pt sample. This deviation is most likely due to thermal diffusion occurring in the film, which is not taken into account in the lumped capacitance thermal model. After this time, the primary source of energy transfer is thermal boundary conductance, and the model and the data agree well. The order of this diffusion time observed in the TTR data in Fig. 3 is in close agreement with diffusion time constants calculated in Table 3. Specifics of diffusion time constant calculations and further analysis are presented in a later section.

With the ultrashort laser pulses used in the TTR measurements, an electron-phonon nonequilibrium is induced in the early part of the TTR data. Using the two temperature model (TTM) to predict the electron-phonon thermalization time with the 10 J m^{-2} incident fluence [32–34], the thermalization time in all the metal films is less than 5.0 ps. Therefore, it is expected that a fast transient spike in the early part of the TTR response due to the electron-phonon nonequilibrium would not affect determining h_{BD} [35]. The result of this nonequilibrium period is a slight rise in lattice temperature due to hot electrons transferring energy to the lattice. Using the TTM with insulated boundary conditions, the predicted lattice temperature rise after electron-phonon equilibration and minimization in the spatial temperature gradient in the film is less than 10 K. Therefore, it should be noted that the actual temperatures of the interfaces could be slightly higher than the prescribed values in the experimental results due to lattice heating.

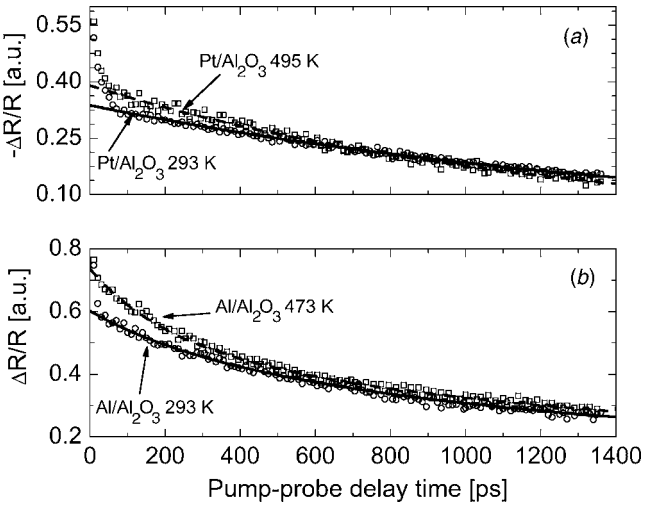

Fig. 3 Thermal model (Eqs. (8)–(14)) fit to TTR data taken on (a) Pt/Al_2O_3 at 293 K and 495 K and (b) Al/Al_2O_3 at 293 K and 473 K. The thermal model is scaled to the TTR data at 200 ps for reasons that will be discussed later in this paper. The TTR data were phase fixed [29] and normalized at the peak reflectance to make clear the differences in the exponential cooling profiles at the different temperatures.

Table 3 Film thermal diffusion times

Material	τ_f at 293 K (ps)	τ_f at T_{max} (ps)
Al	56	62
Cr	86	101
Pt	97	102

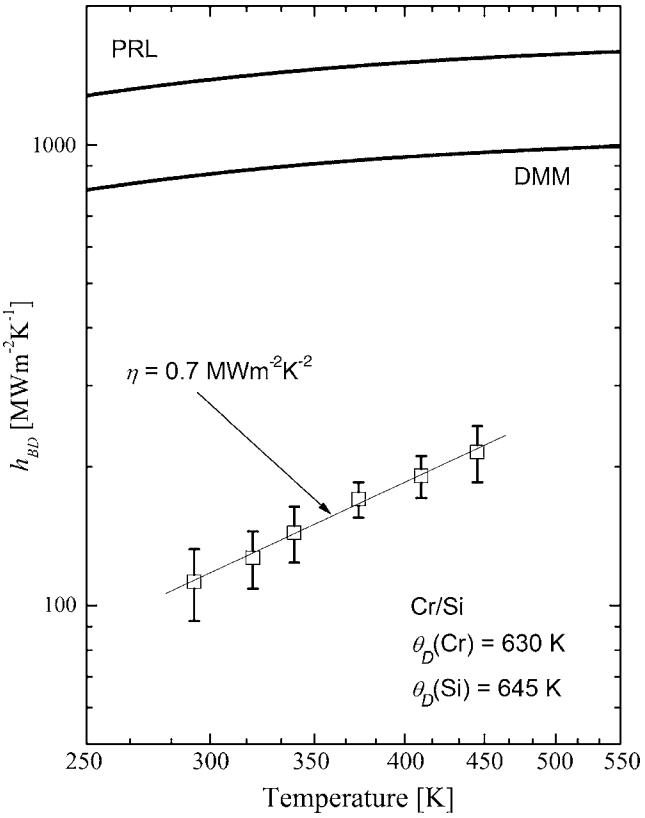

Fig. 4 Thermal boundary conductance data across the Cr/Si interface over a range of temperatures. The data show a linear increase with temperature at a much greater rate than the DMM and PRL.

Experimental Results

The thermal boundary conductances measured from the TTR data are plotted against temperature for the four material systems studied in Figs. 4–7. The line fit to the data depicts the linearity of the relationship between temperature and h_{BD} observed in the experiments. The slope of this line, η, is also presented in these figures along with the Debye temperatures of the materials. In addition, the calculations for the DMM and PRL in these systems are included in these graphs. Figure 4 presents h_{BD} across the Cr/Si interface. In the Cr/Si system, a nearly linear increase of h_{BD} is observed over the temperature range from 293 K to 460 K. Since the highest temperature investigated is less than the θ_D of both the film and substrate, an increase in h_{BD} is expected. However, an 80% increase in h_{BD} occurs over this range, where the DMM and PRL only predict a 15% nonlinear increase that decreases with increasing temperature. The linear temperature dependence may indicate a scattering process that is proportional to

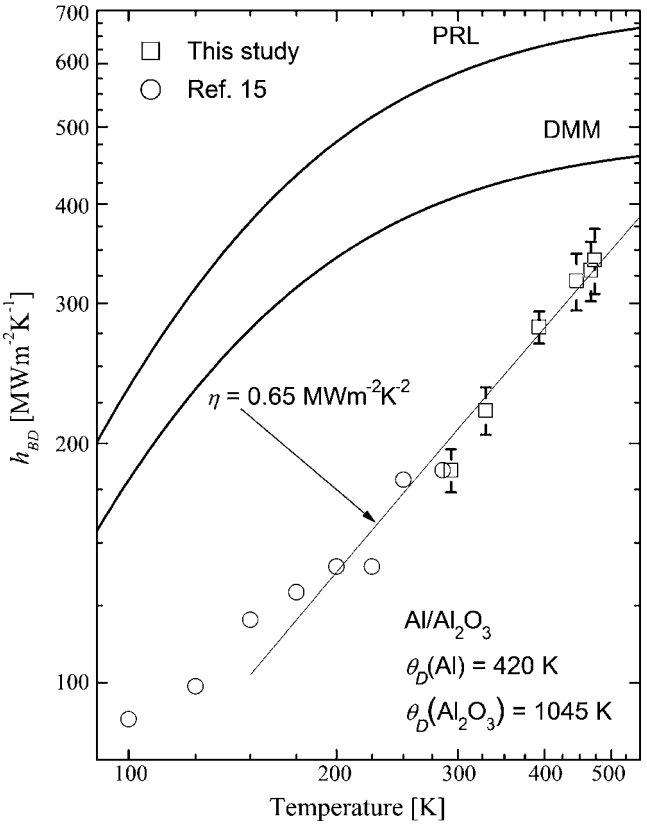

Fig. 5 Thermal boundary conductance data across the Al/Al_2O_3 interface over a range of temperatures. This figure also includes data taken by Stoner and Maris (1993) at low temperatures [15]. The linear trend continues at temperatures higher than the Debye temperature of Al, indicating that inelastic phonon processes could be contributing to h_{BD} at these elevated temperatures.

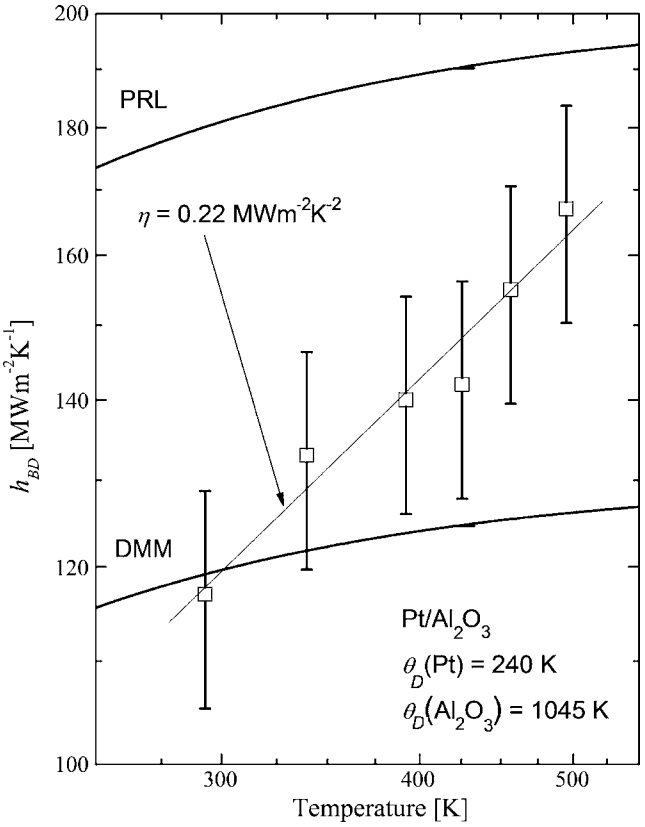

Fig. 6 Thermal boundary conductance data across the Pt/Al_2O_3 interface over a range of temperatures. These temperatures are above the Debye temperature of Pt. According to theory, h_{BD} should not change at temperatures above the Debye temperature of one of the materials assuming only elastic scattering. However, the continued linear increase in measured h_{BD} indicates a contribution from inelastic processes.

increased inelastic scattering events beyond the assumption of single elastic collisions. The change in phonon population with temperature close to and above the Debye temperature is constant, which leads to the temperature independent h_{BD} predictions of the DMM and PRL. However, Cr and Si are very well acoustically matched samples and the deviation associated with measurement repeatability is the largest of any of the samples examined in this work. Although the linear trend with temperature suggests inelastic scattering, there are other transport mechanisms that could also explain the data, which will be discussed in the next section.

Since the change in phonon population is constant with temperatures above and around θ_D, in highly mismatched systems, a continued linear increase of h_{BD} is not expected when the temperature is driven higher than the lower θ_D of the film/substrate material system. With this in mind, Fig. 5 shows the measured h_{BD} across the Al/Al_2O_3 interface. In addition to data measured in this study ($293\ K < T < 500\ K$), low temperature data from Stoner and Maris are included [15]. The linear fit included the data from this study and Stoner and Maris data from 150 K to room temperature. At 150 K, h_{BD} appears to lose its T^3 dependence. Over the temperature range in this study, the experimental data increase by almost 100%, where the DMM only predicts a 10% increase. In addition, the data above the θ_D of Al continue to linearly increase over a 50 K temperature increase. The linear increase above θ_D of Al suggests that multiple-phonon processes may be occurring between single high frequency phonons in the Al_2O_3 and several low frequency phonons in Al. As the temperature was driven above θ_D of Al, the entire phonon population in Al was excited. However, the linear increase of Al_2O_3 phonon population continues and therefore, the increase in h_{BD} above θ_D of Al suggests that h_{BD} is dominated by inelastic scattering. The continued linear trend observed from the data from Stoner and Maris to the high temperature data even above θ_D of Al indicates that there is a smooth transition between regimes where h_{BD} is dominated by elastic and inelastic scattering.

To examine the regime where inelastic scattering would dominate (i.e., temperatures above the Debye temperature of only one of the materials, so that the entire phonon population of one material is excited but not the other), the highly mismatched Pt/Al_2O_3 system was studied. Lyeo and Cahill studied this regime at low temperatures ($T < T_{room}$) with Pb and Bi on diamond [24]. The Al/Al_2O_3 system gives hints toward multiple-phonon processes with the data 50 K above θ_D. However, due to the less than room temperature θ_D of Pt, the highly mismatched Pt/Al_2O_3 shows promising data that further support the findings of inelastic scattering processes in high temperature regimes. Figure 6 shows h_{BD} versus temperature TTR results for Pt/Al_2O_3. The temperature of this interface was increased to over twice θ_D of Pt. Over the investigated temperature range, h_{BD} almost doubles, which is a similar result to the MD calculations that model elastic and inelastic scattering [25].

Similar behavior was observed in the Pt/AlN system over the same temperature range, as seen in Fig. 7. A nearly linear increase in h_{BD} is observed over the temperature range with values approaching the PRL at high temperatures. Aluminum nitride and sapphire have very similar Debye temperatures (Table 1) so similarities in h_{BD} values and temperature trends are expected. The discrepancies in the measured h_{BD} between these two samples

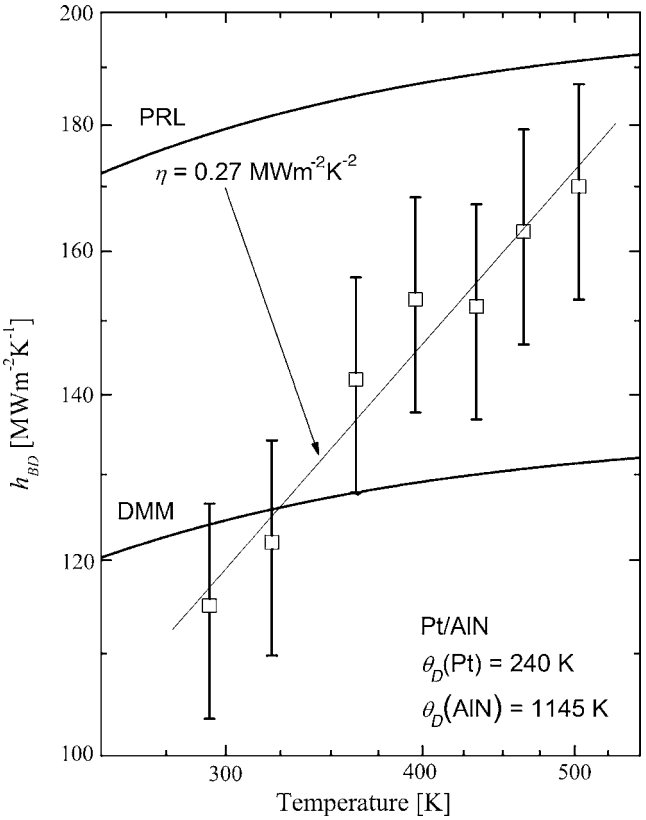

Fig. 7 Thermal boundary conductance data across the Pt/AlN interface over a range of temperatures. A similar linear increase of h_{BD} to the data in Fig. 7 is observed, presenting further evidence toward nonelastic phonon transport channels.

could be due to differences in the physical properties of the boundary or slightly different densities of states not accounted for in the Debye model.

Analysis

The thermal model used to determine h_{BD} from the TTR data (Eqs. (5)–(10)) involves a lumped capacitance assumption in which minimal thermal diffusion is assumed through the film as compared to across the film/substrate interface. Therefore, this model must be scaled to the experimental data at times when the thermal gradient through the film is approximately zero. To estimate this scaling time, the film's thermal diffusion time is approximated from the Fourier number as $\tau_f = d^2/\alpha_f$ [36]. The thermal diffusion times for the films examined in this study are presented in Table 3. These values are calculated with the temperature dependent thermophysical properties of the corresponding bulk material. Since the thicknesses of the samples were chosen to be larger than the mean free path, minimal reduction in thermal conductivity is expected due to size effects [37]. However, to ensure that the model is fit to the data at times when the thermal gradient in the film is minimal, the thermal model was scaled to the TTR data 200 ps after the peak (as shown in Fig. 3), ensuring that even in the unlikely event of a reduction in k_f due to film thickness or quality, the lumped capacitance model can still be correctly applied.

The thermal model is scaled at 200 ps and the thermal model is fit to the 1400 ps of TTR data to extract h_{BD}. In order to check that 1400 ps pump-probe delay is enough time to accurately determine h_{BD} for these samples, the interfacial time constant is estimated as $\tau_{BD} = C_f d/h_{BD}$ [15]. Table 4 lists τ_{BD} for the samples examined in this study using h_{BD} determined from the experiments. The interfacial time constant is less than the 1400 ps TTR scan time for all cases, although it is approaching 1400 ps in the Cr and Pt samples at 293 K. Since this calculation of τ_{BD} is based on bulk properties and is just an estimate, more h_{BD} information could have been extracted from the TTR data with a longer probe delay. This could have lead to measured values of h_{BD} being slightly off around room temperature. However, the room temperature Cr/Si data in this study agree well with previously reported values of h_{BD} on a 50 nm Cr/Si sample subjected to the same deposition conditions as used here and using the same apparatus and same thermal model, but with the data scaled at an earlier time [17]. However, these data are slightly lower than that measured on a 30 nm Cr/Si sample [8]. This 30 nm Cr/Si sample was fabricated differently, however, and fabrication has been shown to cause deviation in h_{BD} [17]. The thermal boundary conductances measured on Pt/Al_2O_3 and Pt/AlN are very close at room temperature (and at all temperatures, for that matter, as previously discussed). Even though Al_2O_3 and AlN have vastly different thermal properties, a similar h_{BD} is expected due to the similar acoustic properties of these materials, giving more confidence in the resolution of h_{BD} of these samples.

Table 4 Interfacial time constants

Material	τ_{BD} at 293 K (ps)	τ_{BD} at T_{max} (ps)
Cr/Si	1342	850
Al/Al_2O_3	924	546
Pt/Al_2O_3	1179	884
Pt/AlN	1286	884

This brings up an important point about the thermal properties used in the model to extract h_{BD} from the TTR data. In this study, bulk properties were used in the analysis. Of specific concern is a reduction in the substrate conductivity due to manufacturing conditions, which could lead to a transient rise in substrate temperature near the interface. When there is a negligible rise in T_s near the interface, the thermal model is weakly dependent on the thermal conductivity of the substrate. However, this dependence increases if the rise in T_s cannot be neglected, which could potentially be a problem in sapphire, which has a relatively low conductivity, leading to a nonexponential decay in the TTR data. The exponential decay in the Pt/Al_2O_3 data shown in Fig. 3 in addition to the similar values for h_{BD} measured on the Pt/Al_2O_3 and Pt/AlN samples elucidates the suitability of the values for the thermal properties used in this study.

Although this study has focused on resolving inelastic scattering processes, other scattering phenomena could be participating in h_{BD} that could influence these results. This is apparent by comparing the predictions of the DMM and PRL to the measured values of h_{BD}; at any given temperature in this study, the DMM and PRL calculations vary by an order of magnitude between the samples while the measured data are all within a factor of 2 of each other. In acoustically well matched material systems, such as Cr and Si, the DMM has been shown to overpredict experimental data when electron-phonon scattering processes occurring near the interface are not taken into account [38]. This scattering process would cause h_{BD} to begin approaching a constant value at lower temperatures. Although this scattering process could explain the overestimation of the h_{BD} by the DMM and PRL for the Cr/Si interface in this study, the linear increase in h_{BD} with temperature observed in Fig. 4 would result from inelastic scattering.

Disorder and mixing around the interface of two materials could lead to multiple-phonon scattering events, which could also influence h_{BD} measurements. These multiple scattering events increase in occurrence with a decrease in phonon mean free path (increase in temperature) [18,19]. Depending on the type of scattering event, different changes in h_{BD} are expected. Multiple elastic scattering events increase h_{BD} in acoustically mismatched

samples but decrease h_{BD} in acoustically matched samples [12]. Assuming an increase in these scattering events with temperature, the Cr/Si h_{BD} would suffer a reduction, while the data in Fig. 4 show an increase, strengthening the conclusion of inelastic scattering. In more heavily mismatched samples (Al/Al_2O_3, Pt/Al_2O_3, Pt/AlN), these multiple elastic scattering events could be contributing in part to the increase in h_{BD} observed over the temperature range. However, MD simulations show this same linear trend at perfect interfaces, which has been attributed to inelastic scattering [25], further supporting the observation of inelastic scattering participating in h_{BD} at high temperatures ($T > \theta_D$).

The experimental data in this study are compared to the DMM and PRL models, which were calculated assuming a Debye density of states. The Debye density of states provides a quick and simple calculation of the DMM and PRL; however, several studies have shown that using a more realistic density of states could significantly change the resulting calculations [39–42]. Recent calculations by Reddy et al. of metal films on semiconductor substrates use the Born von–Karmen model (BKM) to calculate an exact phonon dispersion in the DMM [41]. The more accurate density of states predicted a higher density at lower frequencies and a lower density at higher frequencies as compared to the Debye calculations. This resulted in higher values for the DMM at low temperatures and lower values for the DMM at higher temperatures (i.e., temperatures of interest in this study). With this in mind, the DMM and PRL calculations would decrease from the current results presented in Figs. 4–7. The trend in these calculations (i.e., change in h_{BD} with temperature becomes negligible at temperatures approaching θ_D) also changes with the BKM calculation [41]. With this more realistic density of states, the change in h_{BD} with temperature becomes negligible at much lower temperatures. Applying this conceptual shift to the DMM and PRL data results in an even more drastic difference between the experimental data and the trends in the models assuming only elastic phonon collisions presented in Figs. 4–7. This indicates that inelastic scattering events participating in h_{BD} at higher temperatures are being observed in the experimental data.

The slopes of the linear fit of h_{BD} versus temperature exhibit an interesting trait among the different samples. The slopes of the linear trends (η) as a function of film/substrate Debye temperature ratio (ξ) are shown in Fig. 8 for the Pt data from this study, the Pb/diamond and Bi/diamond data from Lyeo and Cahill [24], and the Au/diamond data from Stoner and Maris [15]. The linear fit to these data is also shown in this figure ($\eta = (1.10\ \mathrm{MW\ m^{-2}\ K^{-2}})\xi$). These specific film/substrate systems are of interest because the majority of the thermal boundary conductances determined in these studies were measured at temperatures above the Debye temperature of the film; therefore, the slopes are representative of the influence of inelastic scattering on h_{BD}. Only the Au/diamond data above 150 K were used for the linear fit to ensure that the reported η for Au/diamond can accurately represent the influence of multiple-phonon processes. The data show an increasing η with increasing ξ, indicating that inelastic processes participating in h_{BD} become more temperature dependent with an increase in acoustic similarity between materials. In samples with greater mismatch (smaller ξ), there exist substrate phonons with much higher frequencies than film phonons, which would have to break down several times to emit phonons with frequencies available in the film's population into the film. However, when the materials become acoustically similar (larger ξ), the decomposition cascade of the substrate phonons is much less severe. Figure 8 indicates that as the film and substrate increase in acoustic similarity, phonon decomposition could be happening more readily. This begins to elucidate the role of inelastic phonon scattering in thermal boundary conductance.

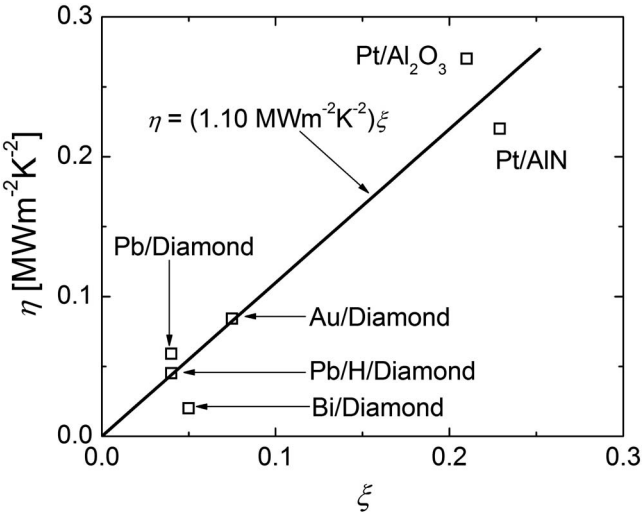

Fig. 8 The slopes of the linear trends (η) as a function of film/substrate Debye temperature ratio (ξ) are shown for the Pt data from this study, the Pb/diamond and Bi/diamond data from Lyeo and Cahill [24], and the Au/diamond data from Stoner and Maris [15]. The linear trends were determined from h_{BD} data measured above the various samples' Debye temperatures to make sure that these slopes represented regimes where inelastic scattering was contributing to h_{BD}. The linear fit to these points is depicted by the solid line. It is apparent that the two materials become acoustically similar (increasing ξ), and inelastic scattering becomes increasingly temperature dependent.

Conclusions

Traditional models for h_{BD} (DMM and PRL) predict thermal boundary conductance at low temperatures ($T \ll T_{room}$, θ_D) relatively well, but at temperatures closer to device operating temperatures these models fail to account for inelastic phonon scattering processes, which can contribute to interface conductance. Previous MD calculations showed strong evidence of inelastic phonon scattering at interfaces at elevated temperatures [25]. To test the effect of these inelastic processes, TTR experiments were performed at elevated temperatures ($T > T_{room}$). The TTR experiments measured the h_{BD} at elevated temperatures on different samples with varying acoustic mismatch. At the temperatures in this study, h_{BD} is assumed to be relatively constant by traditional models considering only elastic scattering. At temperatures around and above the Debye temperature of the metal films, the thermal boundary conductance was shown to increase linearly with temperature, similar to previous MD calculations that take into account inelastic phonon scattering, indicating that multiple-phonon processes are contributing to interfacial transport at high temperatures.

Acknowledgment

The authors would like to thank Rich Salaway, Jennifer Simmons, Thomas Randolph, Jessica Sheehan, and Dr. Mike Klopf for their helpful insight and discussions. This work was funded by the National Science Foundation (CTS-0536744). P.E.H. is greatly appreciative for financial support from the National Science Foundation through the Graduate Research Fellowship Program.

Nomenclature

Bi = Biot number
C = heat capacity, J m^{-3} K^{-1}
d = film thickness, m
h = thermal conductance, W m^{-2} K^{-1}
k = thermal conductivity, W m^{-1} K^{-1}
k_B = Boltzmann's constant, J K^{-1}
M = atomic weight, kg mol^{-1}
q = heat flux, W m^{-2}
T = temperature, K

Greek Symbols

α = thermal diffusivity, m^2 s^{-1}
η = slope of linear fit to h_{BD} temperature data, W m^{-2} K^{-2}
θ_D = Debye temperature, K
ν = acoustic phonon velocity, m s^{-1}
ρ = mass density, kg m^{-3}
τ = diffusion time, s
ξ = ratio of film Debye temperature to substrate Debye temperature
φ = nondimensionalized temperature

Subscripts

BD = boundary
f = film
L = lattice
l = longitudinal branch
s = substrate
t = transverse branch
0 = initial

References

[1] Cahill, D. G., Ford, W. K., Goodson, K. E., Mahan, G. D., Majumdar, A., Maris, H. J., Merlin, R., and Phillpot, S. R., 2003, "Nanoscale Thermal Transport," J. Appl. Phys., **93**, pp. 793–818.
[2] Da Silva, L. W., and Kaviany, M., 2004, "Micro-Thermoelectric Cooler: Interfacial Effects on Thermal and Electrical Transport," Int. J. Heat Mass Transfer, **47**, pp. 2417–2435.
[3] Mahan, G. D., and Woods, L. M., 1998, "Multilayer Thermionic Refrigeration," Phys. Rev. Lett., **80**, pp. 4016–4019.
[4] Phelan, P. E., Song, Y., Nakabeppu, O., Ito, K., Hijikata, K., Ohmori, T., and Torikoshi, K., 1994, "Film/Substrate Thermal Boundary Resistance for an Er–Ba–Cu–O High-Tc Thin Film," ASME J. Heat Transfer, **116**, pp. 1038–1041.
[5] Phelan, P. E., 1998, "Application of Diffuse Mismatch Theory to the Prediction of Thermal Boundary Resistance in Thin-Film High-Tc Superconductors," ASME J. Heat Transfer, **120**, pp. 37–43.
[6] Chen, G., Tien, C. L., Wu, X., and Smith, J. S., 1994, "Thermal Diffusivity Measurement of GaAs/AlGaAs Thin-Film Structures," ASME J. Heat Transfer, **116**, pp. 325–331.
[7] Kim, E.-K., Kwun, S.-I., Lee, S.-M., Seo, H., and Yoon, J.-G., 2000, "Thermal Boundary Resistance at $Ge_2Sb_2Te_5/ZnS:SiO_2$ Interface," Appl. Phys. Lett., **76**, pp. 3864–3866.
[8] Stevens, R. J., Smith, A. N., and Norris, P. M., 2005, "Measurement of Thermal Boundary Conductance of a Series of Metal-Dielectric Interfaces by the Transient Thermoreflectance Technique," ASME J. Heat Transfer, **127**, pp. 315–322.
[9] Swartz, E. T., and Pohl, R. O., 1987, "Thermal Resistances at Interfaces," Appl. Phys. Lett., **51**, pp. 2200–2202.
[10] Cheeke, J. D. N., Ettinger, H., and Hebral, B., 1976, "Analysis of Heat Transfer Between Solids at Low Temperatures," Can. J. Phys., **54**, pp. 1749–1771.
[11] Little, W. A., 1959, "The Transport of Heat Between Dissimilar Solids at Low Temperatures," Can. J. Phys., **37**, pp. 334–349.
[12] Swartz, E. T., and Pohl, R. O., 1989, "Thermal Boundary Resistance," Rev. Mod. Phys., **61**, pp. 605–668.
[13] Cahill, D. G., Bullen, A., and Lee, S.-M., 2000, "Interface Thermal Conductance and the Thermal Conductivity of Multilayer Thin Films," High Temp. - High Press., **32**, pp. 135–142.
[14] Costescu, R. M., Wall, M. A., and Cahill, D. G., 2003, "Thermal Conductance of Epitaxial Interfaces," Phys. Rev. B, **67**, p. 054302.
[15] Stoner, R. J., and Maris, H. J., 1993, "Kapitza Conductance and Heat Flow Between Solids at Temperatures from 50 to 300 K," Phys. Rev. B, **48**, pp. 16373–16387.
[16] Hopkins, P. E., Salaway, R. N., Stevens, R. J., and Norris, P. M., 2006, "Dependence of Thermal Boundary Conductance on Interfacial Mixing at the Chromium-Silicon Interface," *IMECE2006*, Chicago, p. 15288.
[17] Hopkins, P. E., and Norris, P. M., 2006, "Thermal Boundary Conductance Response to a Change in Cr/Si Interfacial Properties," Appl. Phys. Lett., **89**, p. 131909.
[18] Beechem, T., and Graham, S., 2006, "Estimating the Effects of Interface Disorder on the Thermal Boundary Resistance Using a Virtual Crystal Approximation," *Proceedings of the 2006 ASME International Mechanical Engineering Congress*, Anaheim, CA, Paper No. IMECE2006–14161.
[19] Beechem, T. E., Graham, S., Hopkins, P. E., and Norris, P. M., 2007, "The Role of Interface Disorder on Thermal Boundary Conductance Using a Virtual Crystal Approach," Appl. Phys. Lett., **90**, p. 054104.
[20] Snyder, N. S., 1970, "Heat Transport Through Helium II: Kapitza Conductance," Cryogenics, **10**, pp. 89–95.
[21] The term "acoustic mismatch" describes two materials that have significantly different acoustic velocities; the degree of the acoustic mismatch can be easily determined by comparing the materials' Debye temperatures, θ_D.
[22] Chen, Y., Li, D., Yang, J., Wu, Y., Lukes, J., and Majumdar, A., 2004, "Molecular Dynamics Study of the Lattice Thermal Conductivity of Kr/Ar Superlattice Nanowires," Physica B, **349**, pp. 270–280.
[23] Kosevich, Y. A., 1995, "Fluctuation Subharmonic and Multiharmonic Phonon Transmission and Kapitza Conductance Between Crystals With Very Different Vibrational Spectra," Phys. Rev. B, **52**, pp. 1017–1024.
[24] Lyeo, H.-K., and Cahill, D. G., 2006, "Thermal Conductance of Interfaces Between Highly Dissimilar Materials," Phys. Rev. B, **73**, p. 144301.
[25] Stevens, R. J., Zhigilei, L. V., and Norris, P. M., 2007, "Effects of Temperature and Disorder on Thermal Boundary Conductance at Solid-Solid Interfaces: Nonequilbrium Molecular Dynamics Simulations," Int. J. Heat Mass Transfer, **50**, pp. 3977–3989.
[26] Norris, P. M., Caffrey, A. P., Stevens, R. J., Klopf, J. M., Mcleskey, J. T., and Smith, A. N., 2003, "Femtosecond Pump-Probe Nondestructive Examination of Materials," Rev. Sci. Instrum., **74**, pp. 400–406.
[27] Kittel, C., 1996, *Introduction to Solid State Physics*, Wiley, New York.
[28] Hohlfeld, J., Wellershoff, S.-S., Gudde, J., Conrad, U., Jahnke, V., and Matthias, E., 2000, "Electron and Lattice Dynamics Following Optical Excitation of Metals," Chem. Phys., **251**, pp. 237–258.
[29] Stevens, R. J., Smith, A. N., and Norris, P. M., 2006, "Signal Analysis and Characterization of Experimental Setup for the Transient Thermoreflectance Technique," Rev. Sci. Instrum., **77**, p. 084901.
[30] Capinski, W. S., and Maris, H. J., 1996, "Improved Apparatus for Picosecond Pump-and-Probe Optical Measurements," Rev. Sci. Instrum., **67**, pp. 2720–2726.
[31] Ozisik, M. N., 1993, *Heat Conduction*, Wiley, New York.
[32] Anisimov, S. I., Kapeliovich, B. L., and Perel'man, T. L., 1974, "Electron Emission From Metal Surfaces Exposed to Ultrashort Laser Pulses," Sov. Phys. JETP, **39**, pp. 375–377.
[33] Qiu, T. Q., and Tien, C. L., 1992, "Heat Transfer Mechanisms During Short-Pulse Laser Heating on Metals," HTD (Am. Soc. Mech. Eng.), **196**, pp. 41–49.
[34] Smith, A. N., Hostetler, J. L., and Norris, P. M., 1999, "Nonequilibrium Heating in Metal Films: An Analytical and Numerical Analysis," Numer. Heat Transfer, Part A, **35**, pp. 859–873.
[35] Smith, A. N., Hostetler, J. L., and Norris, P. M., 2000, "Thermal Boundary Resistance Measurements Using a Transient Thermoreflectance Technique," Microscale Thermophys. Eng., **4**, pp. 51–60.
[36] Incropera, F., and Dewitt, D. P., 1996, *Fundamentals of Heat and Mass Transfer*, Wiley, New York.
[37] Tien, C. L., Armaly, B. F., and Jagannathan, P. S., 1969, "Thermal Conductivity of Thin Metallic Films and Wires at Cryogenic Temperatures," *Thermal Conductivity VIII*, Plenum, New York.
[38] Majumdar, A., and Reddy, P., 2004, "Role of Electron-Phonon Coupling in Thermal Conductance of Metal-Nonmetal Interfaces," Appl. Phys. Lett., **84**, pp. 4768–4770.
[39] Daly, B. C., Maris, H. J., Imamura, K., and Tamura, S., 2002, "Molecular Dynamics Calculation of the Thermal Conductivity of Superlattices," Phys. Rev. B, **66**, p. 024301.
[40] Young, D. A., and Maris, H. J., 1989, "Lattice-Dynamical Calculation of the Kapitza Resistance Between Fcc Lattices," Phys. Rev. B, **40**, pp. 3685–3693.
[41] Reddy, P., Castelino, K., and Majumdar, A., 2005, "Diffuse Mismatch Model of Thermal Boundary Conductance Using Exact Phonon Dispersion," Appl. Phys. Lett., **87**, p. 211908.
[42] Stevens, R. J., Norris, P. M., and Zhigilei, L. V., 2004, "Molecular-Dynamics Study of Thermal Boundary Resistance: Evidence of Strong Inelastic Scattering Transport Channels," *IMECE2004*, p. 60334.
[43] Levinshtein, M. E., Rumyantsev, S. L., and Shur, M. S., 2001, *Properties of Advanced Semiconductor Materials: GaN, AlN, InN, BN, SiC, SiGe*, Wiley-Interscience, New York.
[44] Fugate, R. Q., and Swenson, C. A., 1969, "Specific Heat of Al_2O_3 From 2 to 25 K," J. Appl. Phys., **40**, pp. 3034–3036.
[45] Gray, D. E., 1972, *American Institute of Physics Handbook*, McGraw-Hill, New York.